CRYSTAL GROWTH & DESIGN

Article

pubs.acs.org/crystal

Mesoporous Materials from Template-Free Vapor-Phase Reductive Leaching of Zn from Zn−M−O Compounds (M = Nb, Mo, W)

Claudia Lermer,[†,‡,§] Megan M. Butala,[†,§] Bethany R. Lettiere,[⊥] and Ram Seshadri*[,†]

[†]Materials Department, Mitsubishi Chemicals Center for Advanced Materials, and Materials Research Laboratory, and [⊥]Department of Mechanical Engineering and Materials Research Laboratory, University of California, Santa Barbara, California 93106, United States

[‡]Department Chemie, Ludwig-Maximilians-Universität München, 81377 München, Germany

ABSTRACT: Vapor-phase leaching of Zn and O from complex oxides was performed with the goal of creating mesoporous metal oxides with connected porosity. At elevated temperatures, complex Zn−M−O oxides (M = Nb, Mo, W) can be reduced to yield textured product materials, including reduced M−O oxides, nitrides, and the metal. The nature of the product varies with temperature, time, reducing atmosphere, and the identity of the metal M. M = Nb results in the formation of porous NbO_2 without the need for extraneous templates or pore formers. The crystal chemistry of the starting Nb compound is found to influence the nature of the texturing or porosity of the final product. The evolution of morphology is also impacted by the starting Zn:Nb ratio. In the case of the Mo and W compounds, reductive leaching yields the metal or metal nitride (for M = Mo). Morphology change is also observed, and varies for each product phase. An additional interesting aspect of the process is that the reductive leaching occurs in stages, allowing intermediate Zn−M−O compositions with reduced M to be stabilized. The evolution of morphology also appears to be dependent on the initial and final crystal structures.

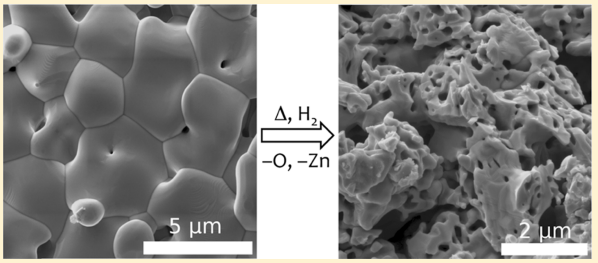

INTRODUCTION

Porosity contributes to the improved performance of materials in applications such as catalysis,[1] liquid chromatography,[2] and energy storage.[3] Various methods have been reported for preparing materials with pores in the 1−200 nm range that are well-suited to many applications.[4,5] Among reported methods are those employing templating agents, which are incorporated into a material and later removed or destroyed, leaving pores whose nature and degree of connectivity are dictated by the template or pore-former. Surfactants,[6] block copolymers,[7] and silica templates[8,9] are among the types of templates commonly used to achieve porosity. One method for inducing porosity without the use of templates is dealloying. An early example of dealloying is Raney nickel, which is porous Ni used for catalysis that is formed by the removal of Al from a Ni−Al alloy.[10] More contemporary examples of inducing porosity by dealloying include the preparations of nanoporous Pt from $Cu_{0.25}Pt_{0.75}$,[11] nanoporous Cu from $Cu_{0.3}Mn_{0.7}$,[12] and porous Sn from Li−Sn alloys.[13] Other studies report the formation of oxides with well-connected pore structures using hydrothermal methods[14,15] and by solid-state decomposition of $Ni(OH)_2$ to NiO.[16]

Vapor-phase leaching of a sacrificial element is another template-free method of achieving porosity that can be used to make porous oxides and metals. Given the mild temperature and pressure conditions required for the volatilization of Zn, reductive leaching of Zn and O from Zn−M−O compounds has been shown to result in a porous oxide for several 3*d* transition metals including M = Mn,[17] Ti,[18,19] and V[19] and porous metals for M = Fe and Ni.[20] In these cases, a Zn−*M*−O precursor compound is heated in a reducing gas, reducing the Zn^{2+} in the complex oxide to the metal, which evaporates from the monolith. Concurrently, some oxygen leaves the monolith as M is reduced to a lower oxidation state. The removal of Zn and O results in a net decrease in the volume of the solid. A typical reaction illustrated for M = Mn is

$$ZnMn_2O_4(s) \xrightarrow{H_2,\Delta} Zn(g) + H_2O(g) + 2MnO(s)$$

For the above reaction, the decrease in the total solid volume is nearly 42% and, under appropriate conditions, this volume loss can be accommodated locally by the formation of connected porosity,[17] rather than by bulk contraction (i.e., densification and sintering). Continued heating of the product at elevated temperatures for an extended period of time would typically be detrimental to the porosity.

Here we report the products of the reductive leaching of Zn and O from Zn−M−O compounds with M = Nb, Mo, and W. Nb was selected on the basis of the possible application of niobium oxides as battery electrode materials,[21−23] and the improvements in electrode performance that accompany porosity and nanoscale features.[24] Monoliths of Nb_2O_5, $ZnNb_2O_6$, and $Zn_3Nb_2O_8$ precursor compounds, with varying Zn:Nb ratios, were prepared and then reduced and leached.

Received: May 1, 2014
Revised: July 14, 2014
Published: August 8, 2014

   dx.doi.org/10.1021/cg500625h | *Cryst. Growth Des.* 2014, 14, 4526−4530

The Zn−Nb−O precursors were selected to evaluate the combined and related effects of crystal structure, Zn:Nb ratio, and volume change on morphology evolution. To consider the effect of transition metal M, the phases and morphologies that resulted from the reductive leaching of $ZnMoO_4$ and $ZnWO_4$ were also studied. Reductive leaching of these compounds led to porosity from $ZnNb_2O_6$, $Zn_3Nb_2O_8$, and $ZnMoO_4$. No fine scale features were evident after the reductive leaching of $ZnWO_4$. In addition to variations in morphology, the nature of the product phase differed according to the transition metal M. Metal oxides resulted for M = Nb and the elemental metal resulted for M = Mo and W.

EXPERIMENTAL SECTION

Dense precursor monoliths of Nb_2O_5, $ZnNb_2O_6$, and $Zn_3Nb_2O_8$ were prepared using solid state methods. Nb_2O_5 was pelletized and sintered in air at 1373 K for 10 h. For the Zn−Nb−O compounds, appropriate molar ratios of ZnO (Sigma-Aldrich 99.0%) and Nb_2O_5 (Sigma-Aldrich 99.9%) were mixed and ground. The resulting powders were pelletized and sintered in air for 10 h at 1398 and 1373 K for $ZnNb_2O_6$ and $Zn_3Nb_2O_8$, respectively.[25] A similar procedure was followed to prepare $ZnMoO_4$ from equal molar ratios of ZnO and MoO_3 (Materion 99.945%) with sintering at 1073 K for 3 h in air.[26] For $ZnWO_4$, equal molar ratios of ZnO and WO_3 (Sigma-Aldrich) were mixed, pelletized, and sintered in air at 1273 K for 3 h.[26]

Thermogravimetric analysis (TGA) using a Cahn TG-2141 TGA in flowing 5% H_2/N_2 tracked mass loss as a function of temperature. This data informed the development of heat treatments by revealing the temperatures at which mass loss associated with Zn and O loss occurs. Nitrogen sorption measurements were performed using a Micro-Meritics TriStar 3000 Porosimeter at 77 K after samples were degassed at 393 K for 12 h under flowing N_2. Laboratory powder X-ray diffraction (XRD) data was collected using Cu Kα radiation (λ = 1.5418 Å) of a Philips X'Pert diffractometer. Rietveld refinement with XND code[27] was used to confirm precursor and product phases. XRD scans were over a 2θ range from 10 to 100°. The morphologies before and after reduction were observed using SEM (XL40 Sirion FEG Digital Scanning Microscope FEI) with a beam voltage of 5 kV. Each sample was mounted on a stainless steel holder using Cu tape and sputtered with Au/Pd to prevent charging. VESTA was used for depicting the crystal structures of precursor and product phases.[28]

RESULTS AND DISCUSSION

Zn−Nb−O. Monoliths of three precursor phases with different Zn:Nb ratios were prepared using solid state methods. Rietveld refinement of X-ray diffraction data confirmed the phase purity of Nb_2O_5, $ZnNb_2O_6$, and $Zn_3Nb_2O_8$ precursor monoliths (Figure 1). Thermogravimetric measurements showed significant mass loss, of Zn and O, near 1123 K. Accordingly, 1123 K was used for reducing heat treatments of Nb compounds. Phase pure NbO_2 reproducibly resulted with reduction from all three precursors in 5% H_2/N_2 at 1123 K for 20 h (Figure 2). That each sample was reduced to the same product phase indicates the stability of NbO_2 at the temperature and atmosphere conditions of the reducing heat treatment.

The precursor monoliths were all sintered and had similarly sized grains (Figure 3a, c, and e). No significant microstructural or morphological changes accompanied the reduction of Nb_2O_5 to NbO_2 (Figure 3a, b). However, connected pores ranging from 150 to 350 nm emerged with the reduction of $ZnNb_2O_6$ to NbO_2 (Figure 3c, d). Connected pores on the order of 100 to 250 nm also resulted from the reductive leaching of Zn and O from $Zn_3Nb_2O_8$ to NbO_2 (Figure 3e, f). Nitrogen sorption measurements of these materials gave inconsistent results of

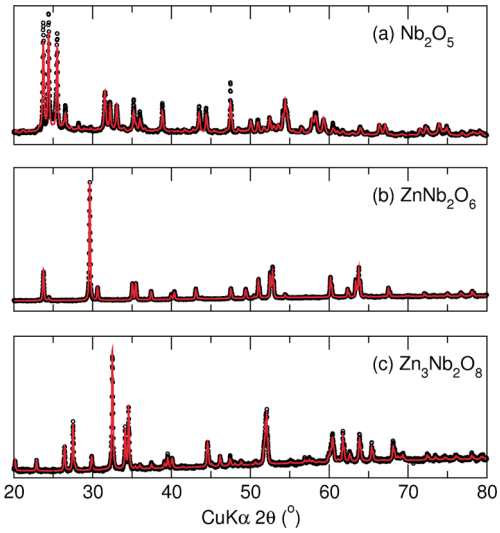

Figure 1. X-ray diffraction confirmed the phase purity of the Nb precursor phases (a) Nb_2O_5, (b) $ZnNb_2O_6$, and (c) $Zn_3Nb_2O_8$. Data as black circles and Rietveld fit in red.

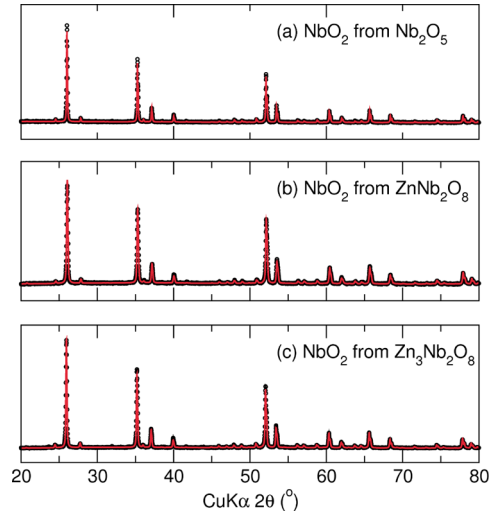

Figure 2. X-ray diffraction confirmed the phase purity of the NbO_2 product phases that resulted from the reduction of (a) Nb_2O_5, (b) $ZnNb_2O_6$, and (c) $Zn_3Nb_2O_8$. Data as black circles and Rietveld fit in red.

both BET surface area and BJH pore size distribution, a consequence of the relatively low surface areas and the too-large pores in these materials.

Although samples with high initial Zn:Nb ratios (3:2 rather than 0:2) had more mass loss with reduction to NbO_2, presumably contributing to the evolution of porous morphology, there are also aspects of atomic arrangement at play. In particular, the anticipated volume change and the relative crystal structures of the precursor and NbO_2 product (Figure 4) can be considered with regard to the emergent morphology. Nb_2O_5 is monoclinic with a combination of tetrahedral and octahedral Nb sites, while monoclinic (defect-rutile) NbO_2 contains all octahedrally coordinated Nb. This transformation involves a mass loss of one O per two Nb atoms and a 28% decrease in volume. $ZnNb_2O_6$ and $Zn_3Nb_2O_8$ precursors, however, have orthorhombic crystal structures with alternating layers of octahedrally coordinated Nb and Zn. Reduction to NbO_2 involves a decrease in volume of 32% and 53%,

dx.doi.org/10.1021/cg500625h | Cryst. Growth Des. 2014, 14, 4526−4530

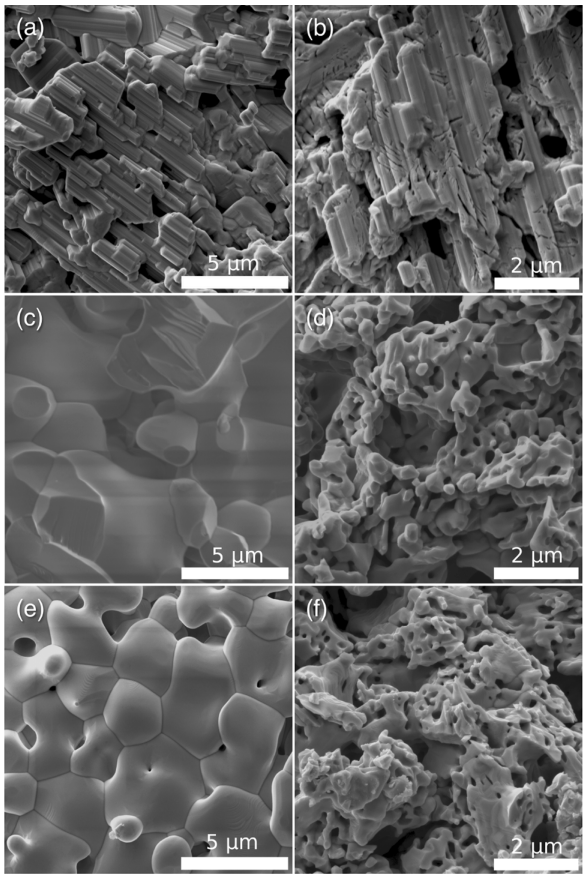

Figure 3. SEM micrographs show that no appreciable microstructural evolution results from the reduction of (a) Nb_2O_5 to (b) NbO_2, but that connected porosity did result from the reduction of dense (c) $ZnNb_2O_6$ and (e) $Zn_3Nb_2O_8$ precursors to (d, f) NbO_2.

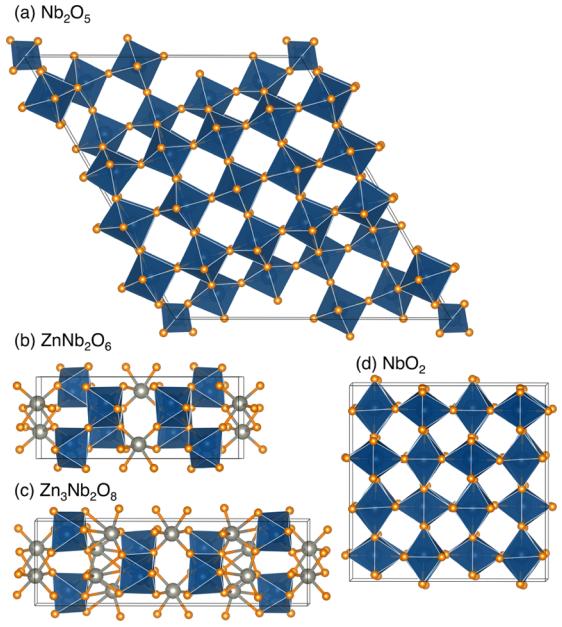

Figure 4. Crystal structures of Nb compounds: (a) Monoclinic Nb_2O_5 projected down the *b* axis. (b) Orthorhombic $ZnNb_2O_6$ projected down the *c* axis. (c) Orthorhombic $Zn_3Nb_2O_8$ projected down the *c* axis. (d) Monoclinic NbO_2 projected down the *b* axis. NbO_n polyhedra are blue, Zn is gray, and O is orange.

respectively. The alternating sheets of Nb and Zn likely provide good diffusion paths for metallic Zn out of the structure, in the same way Li easily diffuses between the layers of a Li_xCoO_2 intercalation battery cathode.

Zn−Mo−O. To assess the effect of transition metal M on reductive leaching, $ZnMoO_4$ precursor monoliths were prepared using solid-state methods. The phase purity was confirmed using XRD and Rietveld refinement (Figure 5a).

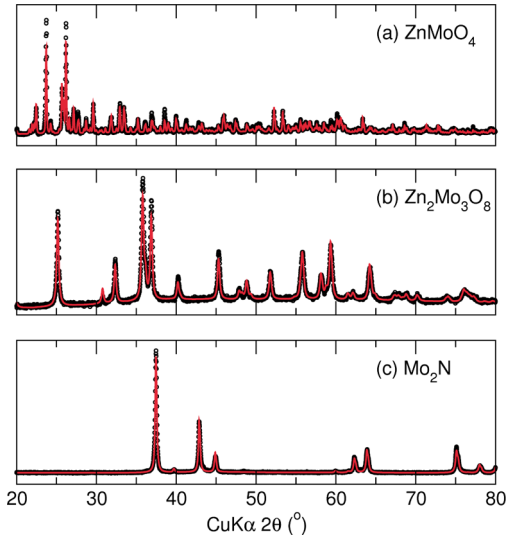

Figure 5. X-ray diffraction was used to confirm the preparation of (a) $ZnMoO_4$ and to identify the reductive leaching products (b) $Zn_2Mo_3O_8$ from reduction at 923 K for 4 h in 5% H_2/N_2 and (c) Mo_2N at 1123 K for 4 h in 5% H_2/N_2. Data as black circles and Rietveld fit in red.

Reduction at several time and temperature combinations led to the formation of different phases. Heating in 5% H_2/N_2 at 923 K for 4 h resulted in the formation of phase pure $Zn_2Mo_3O_8$ with only some Zn removal and the reduction of Mo^{6+} to Mo^{4+} (Figure 5b), providing a new synthesis route for this compound. For reductions between 973 and 1073 K, a combination of $Zn_2Mo_3O_8$ and Mo_2N resulted. Reduction at 1123 K for 4 h in 5% H_2/N_2 resulted in phase pure Mo_2N (Figure 5c), in which all of the Zn and O were removed. Repeating the reduction at 1123 K for 4 h in 5% H_2/Ar formed Mo metal.

The phase change to each Mo product phase was accompanied by a microstructural or morphological change. Dense $ZnMoO_4$ (Figure 6a) reduced at 923 K to the intermediate $Zn_2Mo_3O_8$ developed a platelike morphology at the surface (Figure 6b). Reduction at 1123 K resulted in the complete removal of Zn, forming Mo_2N in 5% H_2/N_2 and textured Mo metal in 5% H_2/Ar (Figure 6c, d), both with connected pores in the 50 to 100 nm range, as assessed by SEM. Although these pore sizes are within the range of nitrogen sorption, neither BET surface area nor BJH pore size distribution were reliable for these low-surface-area materials.

The evolution of morphology and microstructure with increasing Zn volatilization is observed in Figure 6. Once again, rather than considering the mass loss associated with Zn and O removal, the emergence of features can be considered in terms of the atomic arrangement of each reduction product phase relative to the $ZnMoO_4$ precursor (Figure 7). $ZnMoO_4$ has octahedrally coordinated Zn and tetrahedrally coordinated

dx.doi.org/10.1021/cg500625h | *Cryst. Growth Des.* 2014, 14, 4526−4530

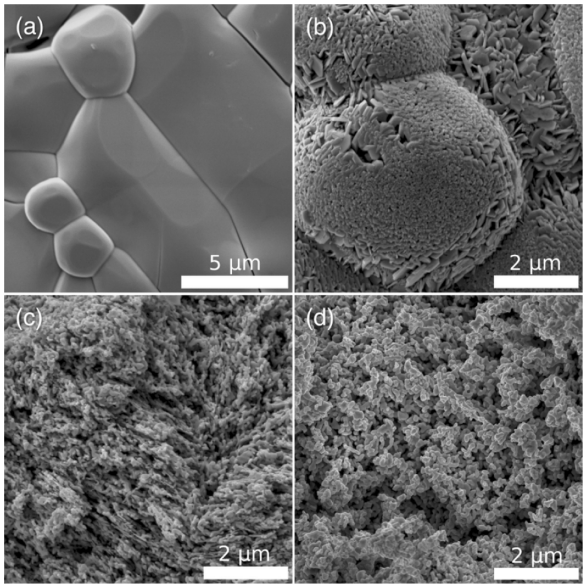

Figure 6. SEM shows that the dense precursor (a) $ZnMoO_4$ forms (b) a platelike morphology with reduction to $Zn_2Mo_3O_8$ at 923 K for 4 h in 5% H_2/N_2. Connected pores on the order of 50 to 100 nm were observed after reduction to (c) Mo_2N at 1123 K in 5% H_2/N_2 and (d) Mo at 1123 K in 5% H_2/Ar.

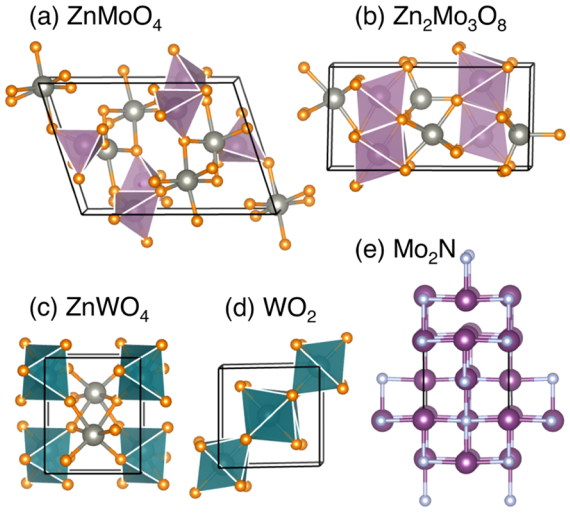

Figure 7. Crystal structures of Mo and W compounds: (a) Triclinic $ZnMoO_4$ projected down the *c* axis. (b) Hexagonal $Zn_2Mo_3O_8$ projected down the *b* axis. (c) Monoclinic $ZnWO_4$ projected down the *c* axis. (d) Monoclinic WO_2 projected down the *c* axis. (e) Tetragonal Mo_2N projected down the *a* axis. MoO_n polyhedra are purple, WO_n polyhedra are green, Zn is gray, and O is orange.

Mo. With the first removal of Zn, there is a transformation to $Zn_2Mo_3O_8$, which has alternating layers of ZnO_6 and MoO_6 octahedra, with retention of some ZnO_4 tetrahedra (Figure 7). This first transformation has a decrease in volume near 45% . An additional 36% volume decrease results from the reduction of $Zn_2Mo_3O_8$ to Mo. The net volume loss is significant, and, in this case, manifests with the emergence of texture or connected porosity, respectively, in reduction products.

Zn−W−O. The $ZnWO_4$ precursor was prepared using solid state methods. Precursor and reduction product phases were assessed using powder XRD (Figure 8). A biphasic product of WO_2 and W resulted from the reduction of $ZnWO_4$ at 1073 K

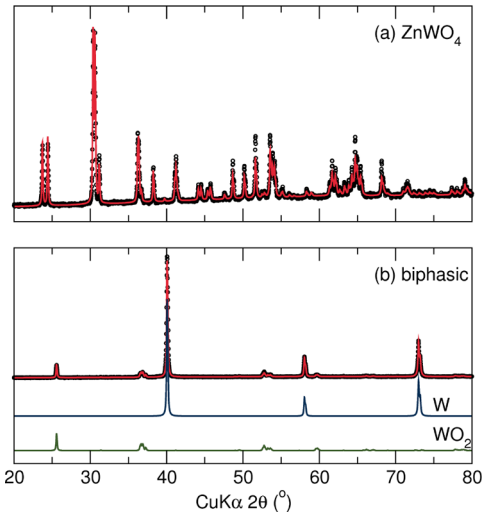

Figure 8. X-ray diffraction was used to confirm the preparation of (a) $ZnWO_4$ and identify the product phases. Reduction at 1073 K for 3 h in 5% H_2/N_2 resulted in (b) biphasic W (blue) and WO_2 (green). Increasing the reducing time led to complete reduction to W metal. Data as black circles and Rietveld fit in red.

for 3 h in 5% H_2/N_2. A 10 h reduction using the same temperature and reducing gas resulted in pure W.

As observed for systems with M = Nb and Mo, the removal of Zn saw a change in morphology for M = W. The dense, monoclinic $ZnWO_4$ did increase in texture with reduction to a combination of *bcc*-W and monoclinic WO_2. Longer reduction, however, saw complete reduction to W metal, which appeared to have faceted grains (Figure 9) rather than more distinct

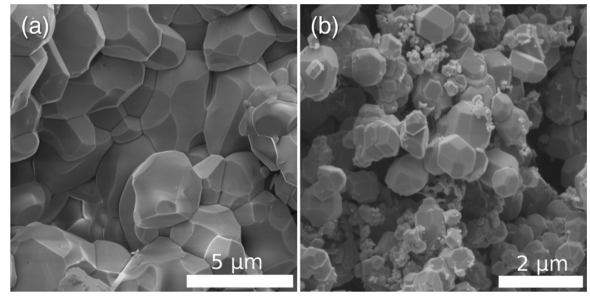

Figure 9. SEM reveals (a) the dense morphology of the $ZnWO_4$ precursor and (b) the faceted grains of W that result from complete Zn vaporization and reduction at 1023 K for 10 h.

features observed for M = Nb and Mo. The crystal structure of $ZnWO_4$ is comparable to that of $ZnNb_2O_6$, with alternating layers of Zn and W octahedra (Figure 7). Based on the structures, the expected volume change with reduction is about 50% for the transition from $ZnWO_4$ to WO_2 and 76% for the transition from $ZnWO_4$ to W. Despite the significant volume change with reduction, the volume loss in this case manifests in the formation of faceted grains.

CONCLUSION

The use of reductive leaching of Zn and O from Zn−M−O compounds with M = Nb, Mo, and W to prepare porous and textured metals and oxides has been presented. Porous NbO_2 resulted from the reductive leaching of $ZnNb_2O_6$ and $Zn_3Nb_2O_8$, but not from Nb_2O_5. This is in contrast to what

dx.doi.org/10.1021/cg500625h | Cryst. Growth Des. 2014, 14, 4526−4530

has been previously reported for the reduction of Mn_3O_4 to MnO, during which pores develop.[29] Mo or Mo_2N with connected porosity resulted from the reductive leaching of Zn from $ZnMoO_4$, depending on the reducing atmosphere. An intermediate $Zn_2Mo_3O_8$ with platelike morphology resulted with some Zn removal. W metal from the $ZnWO_4$ precursor does not show such microstructural or morphological development, but has faceted, micron-sized grains. The chemical composition (metal, oxide, or nitride) of the resulting phase varied according to the nature of M, specifically on the stability of M relative to its oxides (or nitride).

AUTHOR INFORMATION

Corresponding Author

*E-mail: seshadri@mrl.ucsb.edu.

Author Contributions

[§]Authors C.L. and M.M.B. contributed equally to this work

Notes

The authors declare no competing financial interest.

ACKNOWLEDGMENTS

Fellowship support to MMB from the ConvEne IGERT Program (NSF-DGE 0801627) is gratefully acknowledged. CL gratefully acknowledges support from the IMI Program of the National Science Foundation under Award No. DMR 0843934, and the UCSB-MPG Program for International Exchange in Materials Science. Research reported here made use of MRL Central Facilities, supported by the MRSEC Program of the NSF under Award DMR 1121053.

REFERENCES

(1) Corma, A.; Nemeth, L. T.; Renz, M.; Valencia, S. *Nature* **2001**, *412*, 423−425.
(2) Grun, M.; Kurganov, A. A.; Schacht, S.; Schuth, F.; Unger, K. K. *J. Chromatogr. A* **1996**, *740*, 1−9.
(3) Jiao, F.; Bao, J.; Hill, A. H.; Bruce, P. G. *Angew. Chem.* **2008**, *120*, 9857−9862.
(4) Erlebacher, J.; Seshadri, R. *MRS Bull.* **2009**, *34*, 561−566.
(5) Shoemaker, D. P.; Corr, S. A.; Seshadri, R. *Mater. Res. Soc. Symp. Proc.* **2009**, *1148E*, PP10−01.
(6) Kresge, C.; Leonwicz, M.; Roth, W.; Vartuli, J. C.; Beck, J. S. *Nature* **1992**, *359*, 710−712.
(7) Zhao, D.; Feng, J.; Huo, Q.; Melosh, N.; Fredrickson, G. H.; Chmelka, B. F.; Stucky, G. D. *Science* **1998**, *279*, 548−552.
(8) Han, Y.-J.; Kim, J. M.; Stucky, G. D. *Chem. Mater.* **2000**, *12*, 2068−2069.
(9) Hou, R. Z.; Ferreira, P.; Vilarinho, P. M. *Cryst. Growth Des.* **2011**, *11*, 5215−5220.
(10) Raney, M. U.S. Patent 1 563 787, 1925.
(11) Pugh, D.; Dursun, A.; Corcoran, S. *J. Mater. Res.* **2003**, *18*, 216−221.
(12) Chen, L.-Y.; Yu, J.-S.; Fujita, T.; Chen, M.-W. *Adv. Funct. Mater.* **2009**, *19*, 1221−1226.
(13) Chen, Q.; Sieradzki, K. *Nat. Mater.* **2013**, *12*, 1102−1106.
(14) Ding, N.; Liu, S.; Feng, X.; Gao, H.; Fang, X.; Xu, J.; Tremel, W.; Lieberwirth, I.; Chen, C. *Cryst. Growth Des.* **2009**, *9*, 1723−1728.
(15) Chen, K.; Noh, Y. D.; Li, K.; Komarneni, S.; Xue, D. *Cryst. Growth Des.* **2013**, *117*, 10770−10779.
(16) Shukla, A. K.; Ercius, P.; Gautam, A. R. S.; Cabana, J.; Dahmen, U. *Cryst. Growth Des.* **2014**, *14* (5), 2453−2459.
(17) Toberer, E. S.; Seshadri, R. *Adv. Mater.* **2005**, *17*, 2244−2246.
(18) Toberer, E. S.; Epping, J. D.; Chmelka, B. F.; Seshadri, R. *Chem. Mater.* **2006**, *18*, 6345−6351.
(19) Yang, M.; MacLeod, M. J.; Tessier, F.; DiSalvo, F. J. *J. Am. Ceram. Soc.* **2012**, *95*, 3084−3089.
(20) Toberer, E. S.; Joshi, A.; Seshadri, R. *Chem. Mater.* **2005**, *17*, 2142−2147.
(21) Kumagai, N.; Ishiyama, I.; Tanno, K. *J. Electrochem. Soc.* **1999**, *146*, 3203−3210.
(22) Kumagai, N.; Koishikawa, Y.; Komaba, S.; Koshiba, N. *J. Electrochem. Soc.* **1999**, *146*, 3203−3210.
(23) Li, H.; Balaya, P.; Maier, J. *J. Electrochem. Soc.* **2004**, *151*, A1878−A1885.
(24) Bruce, P.; Scrosati, B.; Tarascon, J. *Angew. Chem., Int. Ed.* **2008**, *47*, 2930−2946.
(25) Noh, T.; Cho, I.; Lee, S.; Kim, D. W.; Park, S.; Seo, S. W.; Lee, C. W.; Hong, K. S. *J. Am. Ceram. Soc.* **2012**, *95*, 227−231.
(26) Kim, E.; Jeon, C.; Clem, P. *J. Am. Ceram. Soc.* **2012**, *95*, 2934−2938.
(27) Berar, J.-F.; Garnier, P. *NIST Spec. Publ.* **1992**, *846*, 212.
(28) Momma, K.; Izumi, F. *J. Appl. Crystallogr.* **2011**, *44*, 1272−1276.
(29) Toberer, E. S.; Schladt, T. D.; Seshadri, R. *J. Am. Chem. Soc.* **2006**, *128*, 1462−1463.